TU Delft

Delft University of Technology

Thermal Infrared Imaging of the Urban Landscape to Understand Urban Microclimate

Yang, Jinxin; Menenti, Massimo; Wong, Man S.; Wu, Zhifeng; Ouyang, Xiaoying; Xu, Yong; Abbas, Sawaid

DOI
10.1002/9781119625865.ch17

Publication date
2021

Document Version
Final published version

Published in
Urban Remote Sensing

Citation (APA)
Yang, J., Menenti, M., Wong, M. S., Wu, Z., Ouyang, X., Xu, Y., & Abbas, S. (2021). Thermal Infrared Imaging of the Urban Landscape to Understand Urban Microclimate. In X. Yang (Ed.), *Urban Remote Sensing: Monitoring, Synthesis, and Modeling in the Urban Environment, Second Edition* (pp. 369-389). Wiley. https://doi.org/10.1002/9781119625865.ch17

Important note
To cite this publication, please use the final published version (if applicable).
Please check the document version above.

Copyright
Other than for strictly personal use, it is not permitted to download, forward or distribute the text or part of it, without the consent of the author(s) and/or copyright holder(s), unless the work is under an open content license such as Creative Commons.

Takedown policy
Please contact us and provide details if you believe this document breaches copyrights.
We will remove access to the work immediately and investigate your claim.

This work is downloaded from Delft University of Technology.
For technical reasons the number of authors shown on this cover page is limited to a maximum of 10.

Green Open Access added to TU Delft Institutional Repository

'You share, we take care!' - Taverne project

https://www.openaccess.nl/en/you-share-we-take-care

Otherwise as indicated in the copyright section: the publisher is the copyright holder of this work and the author uses the Dutch legislation to make this work public.

Thermal Infrared Imaging of the Urban Landscape to Understand Urban Microclimate

CHAPTER 17

Jinxin Yang[1], Massimo Menenti[2], Man S. Wong[3], Zhifeng Wu[1], Xiaoying Ouyang[4], Yong Xu[1], and Sawaid Abbas[5]

[1]*School of Geography and Remote Sensing, Guangzhou University, Guangzhou, China*

[2]*Faculty of Civil Engineering and Earth Sciences, Delft University of Technology, GA Delft, The Netherlands*

[3]*Department of Land Surveying and Geo-Informatics, The Hong Kong Polytechnic University, Hong Kong, China*

[4]*State Key Laboratory of Remote Sensing Science, Institute of Remote Sensing and Digital Earth, Chinese Academy of Sciences, Beijing, China*

[5]*Department of Land Surveying and Geo-Informatics, Hong Kong Polytechnic University, Kowloon, Hong Kong*

Abstract

Thermal remote sensor data have been widely used in urban climate and environmental research. The urban geometry, however, hinders a nadir-looking radiometer to observe all urban facets, which makes the observed urban radiometric surface temperature (T_r) different from the urban complete surface temperature (T_c). The T_c of all urban facets conveys complete information on the response of the urban surface to radiometric and convective forcing. In this chapter, we firstly examined the limitations of three current most popular surface temperature retrieval methods for radiometric surface temperature retrieval. Then, we discussed a methodology using precisely designed numerical experiments through an urban micro-climate model to help understand thermal radiative transfer within the built-up space and the relationship between observed T_r and T_c. Specifically, T_r is firstly retrieved from radiance observed at the top of atmosphere over urban areas by applying corrections for atmospheric and emissivity effects. Numerical experiments are designed to evaluate different combinations of urban geometry with the configuration of radiometric observations to construct the relationships between T_r and T_c. Finally, T_c is estimated by using such relationships. T_c can then be used for urban climate and

Urban Remote Sensing: Monitoring, Synthesis, and Modeling in the Urban Environment, Second Edition. Edited by Xiaojun Yang.
© 2022 John Wiley & Sons Ltd. Published 2022 by John Wiley & Sons Ltd.

environment research. We further present a case study to demonstrate the methodology discussed above, which was based on the estimation of T_c from satellite TIR data under the condition that the urban areas have no vegetation or negligible vegetation. Lastly, we discussed some challenges that need to be addressed in the future for improving the applicability of thermal infrared remote sensing in urban areas.

17.1 INTRODUCTION

17.1.1 URBAN MICROCLIMATE AND SURFACE ENERGY BALANCE

Urban surface energy balance determines the urban climate (Oke 1988; Voogt and Oke 2003; Nazarian et al. 2018; Arnfield 2003; Morrison et al. 2018). Conversion of natural surfaces into impervious urban areas reduces evaporation and transpiration and further decreases the mitigating potential of ambient temperature in rapidly urbanizing landscapes (Oke 1982). Thus, the higher absorbed energy by the impervious surfaces the surface temperature, leading to higher emittance and increased dissipation as sensible heat flux, which warms the atmospheric boundary layer. Thus, urban surface temperature (UST) is the result of urban surface energy balance. The difference between urban and rural surface energy balance, especially in the contributing energy fluxes, tends to make the UST higher than rural surface temperature which is known as surface urban heat island (SUHI).

UST is an important indicator of urban climate, which is largely affected by urban geometric and material characteristics because they affect the urban surface energy exchange. These characteristics control numerous processes which directly or indirectly influence the exchange of convective and radiative fluxes. Geometric characteristics of urban landscape impact the visibility of the open sky and thus alter the exchange of the longwave and shortwave radiative flux between the urban landscape and the atmosphere (Rizwan et al. 2008). In addition, the geometric characteristics in urban areas also affect convective heat dissipation due to the change of aerodynamic resistance. Typical parameterization methods of urban surface energy balance include single-source and dual-source models. Dual-source models separate the mixed pixels into vegetation and impervious surface components. However, the inherent 3D nature of a multi-facet urban geometric model makes it difficult to ascertain the energy exchange by using the conventional single or dual source models (Voogt and Grimmond 2000; Kanda et al. 2005, 2007; Xu et al. 2008). Different facets of the urban surface contribute to meteorological processes differently and all facets of the urban surface area are involved in the urban land surface processes and energy exchange and should be considered. Thus, the parameterization of urban surface energy exchange should consider all facets of urban areas. Each component facet temperature and complete surface temperature, defined by Voogt and Oke (1997) as the average temperature of the total active surface area, are useful for urban climate and surface energy balance studies. The observation of the complete surface temperature can be challenging since the temperature of all component facets is required. Therefore, some practical approximations, such as the radiometric observation of the surface temperature, may need to be explored.

17.1.2 RADIOMETRIC SURFACE TEMPERATURE OBSERVED BY REMOTE SENSING (T_r)

Radiometric measurements from a space- or airborne platform provide plenty of useful and real information about the land surface at different temporal and spatial scales. Surface temperature of natural surface can be retrieved from the data observed by remote sensing after

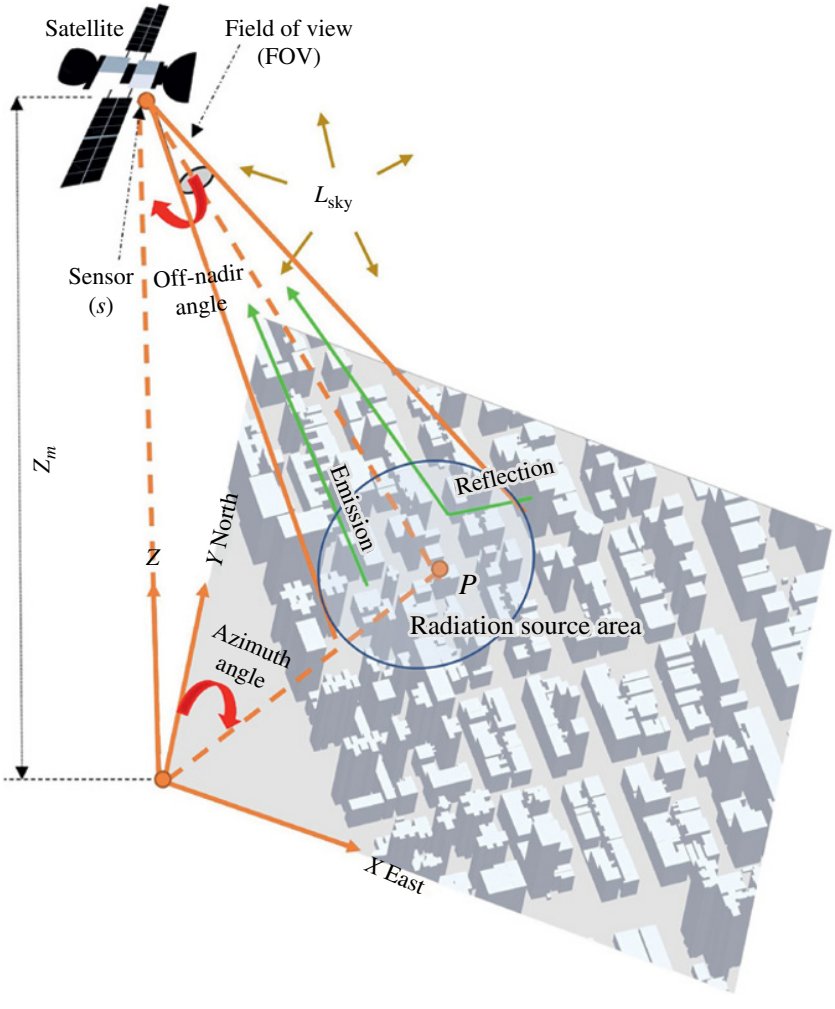

FIGURE 17.1 Radiation source area of a remote sensor that receives radiance emitted by and reflected from an urban area. *Source*: Adapted from Oke et al. (2017).

atmospheric and emissivity corrections (Becker and Li 1995), and methods to retrieve the surface temperature have been reviewed elsewhere (Li et al. 2013). The UST directly retrieved from remote sensing after atmospheric and emissivity correction is defined as urban canopy radiometric surface temperature (T_r). Remote sensing observations of urban space are constrained by the urban geometry, and space-borne, nadir-looking thermal imaging radiometers do not capture all facets of urban features playing a significant role in radiation exchange (Roth et al. 1989; Jiang et al. 2018; Adderley et al. 2015). The observed exitance from an urban canopy depends on the observation direction and the urban geometry as shown in Figure 17.1. Although T_r does not capture information on all facets, it includes the information from roofs and ground (e.g. road) and the radiation reflected by ground and roofs originally emitted by building walls and by the atmosphere (Figure 17.1). The reflected part of radiation depends on the wall surface temperature and material emissivity of wall and road as well as the sensor-ground geometry. The T_r retrieval method can be found in Section 17.2.1.

17.1.3 COMPLETE SURFACE TEMPERATURE (T_c)

Urban thermal heterogeneity and 3D geometry, combined with the observation direction, lead to observed thermal anisotropy. This severely affects mapping of UST and then the understanding of urban climate indicators such as SUHI (Hu and Brunsell 2013; Zhan et al. 2012; Li and Li 2020; Wang et al. 2018; Wang and Chen 2019). The impact of urban geometry and surface heterogeneity on the application of thermal infrared remote sensing for urban climate research was highlighted by Roth et al. (1989) and then further examined by Voogt and Oke (1997, 1998, 2003). Voogt and Oke (1997) introduced the complete surface temperature defined as the average temperature of the total active surface area (Eq. 17.1 and Figure 17.1). Voogt and Oke (1998) documented the impact of anisotropy on the thermal infrared exitance of selected urban targets. Voogt and Oke (2003) reviewed the state of the art of thermal infrared remote sensing of urban landscapes. These studies suggest that the complete surface temperature, which captures all the facet temperatures, is a more meaningful variable for urban climate research since it includes the information on all facets that is needed to derive the radiative and convective fluxes in the built-up environment.

As Figure 17.2 shows, the urban space is a 3D area with complex geometric characteristics. The complete UST T_c of urban space was defined by Voogt and Oke (1997) as the average temperature of all facets of urban space weighted by the surface area of each facet, including building and vegetation (Eq. 17.1):

$$T_c = \sum_{i=1}^{n} A_i T_i \tag{17.1}$$

Ai is the component area fraction, and *Ti* is the component temperature (Rooftop, wall facet, road, and vegetation). By definition, T_c is not directly observable by a nadir-looking space- or

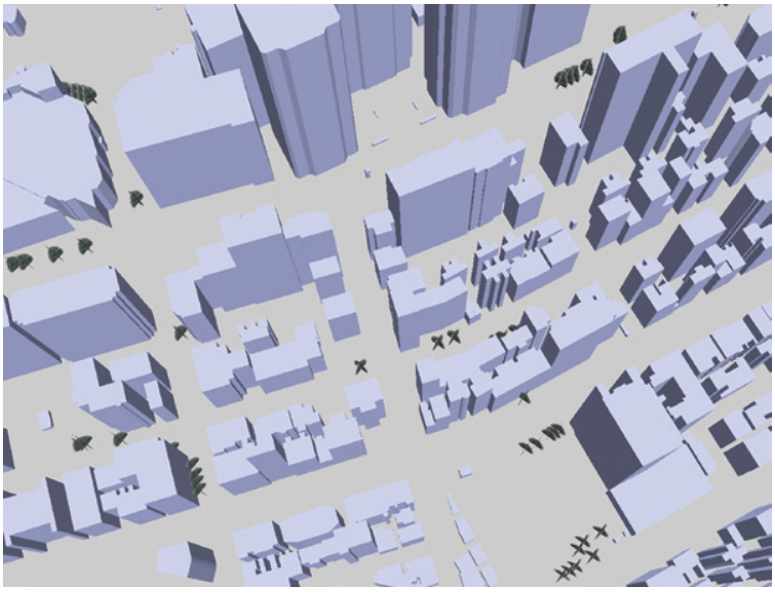

FIGURE 17.2 Urban space with 3D geometry.

airborne imaging radiometer. Under limited assumptions, T_c can be estimated by hemispherical or wide FOV (field of view) radiometers measuring upwelling longwave radiation (Voogt and Oke 1997).

17.1.4 LINK BETWEEN T_r AND T_c

Many researchers have used high-spatial-resolution data from ground and/or airborne platforms to estimate T_c by taking into account the thermal heterogeneity of urban landscapes (Voogt and Oke 1997; Jiang et al. 2018; Allen et al. 2018). Thermal heterogeneity due to the mixed emittance by different elements of the urban landscape, e.g. road and roof facets in the same pixel, limits the accurate estimation of T_c from low resolution thermal infrared images. Estimating T_c from T_r, retrieved from TOA (top of atmosphere) radiometric data acquired by space-borne imaging radiometers, is attractive because of the spatial and temporal coverage, although the spatial resolution of current observation systems is not sufficient to capture the urban landscape with sufficient details. When a pixel is thermally homogeneous, all facets have the same temperature and the T_c is equal to the radiometric temperature observed by remote sensing. On the other hand, the radiometric temperature does not represent the complete temperature in pixels which are not thermally homogenous, since the radiometric temperature is retrieved from the exitance which does not include emittance by all facets of the urban space (Yang et al. 2020). Multiple factors determine the thermal heterogeneity and the relationship between T_r and T_c. The complex geometric and material characteristics of buildings and vegetation make the energy exchange vary within the urban space. In addition, the solar position affects the shadow and sunlit distribution within the pixel. Both of them determine the radiative forcing and thermal heterogeneity (Yang et al. 2016). The thermal heterogeneity makes the parameterization of bulk radiative and convective fluxes complex and makes the difference between T_c and T_r to vary across the urban space (Krayenhoff and Voogt 2016). In summary, the determinant factors of thermal heterogeneity include structural/morphological factors, solar position, material properties, and boundary layer conditions (Krayenhoff and Voogt 2016). A link between T_c and T_r can be constructed by applying the observations of these variables.

To apply thermal infrared remote sensing to observe urban processes, the issue of connecting the radiometric UST detected by a remote sensing instrument and the real UST within the urban canopy must be addressed. To address this issue, numerical experiments with an urban microclimate numerical model can help understand the drivers of urban energy exchange and thermal heterogeneity. In addition, when thermal images are used to understand urban climate and energy exchange, we need to consider the geometry and material heterogeneity.

The following sections discuss the basic methodology for T_r retrieval and T_c estimation and present the results of a case study, along with a discussion on the perspectives toward further development of urban thermal infrared remote sensing.

17.2 METHODOLOGY

17.2.1 RETRIEVAL OF RADIOMETRIC SURFACE TEMPERATURE (T_R)

The radiance in the infrared wavebands measured by a spaceborne sensor is the TOA radiance, which can be described as (Li et al. 2013):

$$I_\lambda(i) = E_\lambda(i)\tau_\lambda(i) + R_{at\uparrow}(i) \tag{17.2}$$

where $E_\lambda(i)$ ($W \cdot m^{-2} \cdot sr^{-1} \cdot \mu m^{-1}$) is the channel radiance of pixel i at the channel central wavelength λ and observed at the top of the urban canopy, $\tau_\lambda(i)$ is the effective atmospheric transmittance at the wavelength λ, and $R_{at\uparrow}(i)$ is the upward thermal radiance of atmosphere ($W \cdot m^{-2} \cdot sr^{-1} \cdot \mu m^{-1}$) (Li et al. 2013).

For a flat urban surface, the complex geometric effects can be neglected and the surface leaving thermal radiance is

$$E_\lambda(i) = \varepsilon_\lambda(i) B_\lambda\left(T_r(i)\right) + \left(1 - \varepsilon_\lambda(i)\right) * R_{at}^{\downarrow}(i) \tag{17.3}$$

where $\varepsilon_\lambda(i)$ is the material emissivity of pixel i, B is the Planck function, $T_r(i)$ is the radiometric surface temperature of pixel i, and $R_{at}^{\downarrow}(i)$ is the downward radiance from the atmosphere.

Retrieval of radiometric temperature from the radiance leaving from the urban canopy is significantly influenced by the emissivity. When the emissivity is known, the radiometric surface temperature ($T_r(i)$) can be calculated from the ground leaving radiance after emissivity correction by inverting Planck's law:

$$T_r(i) = B^{-1}\left(B_\lambda\left(T_r(i)\right)\right) = \frac{C_2}{\lambda \cdot \ln\left[\left(\frac{C_1}{\lambda^5 \frac{E_\lambda(i) - \left(1 - \varepsilon_\lambda(i)\right) * R_{at}^{\downarrow}(i)}{\varepsilon_\lambda(i)}}\right) + 1\right]} \tag{17.4}$$

C_1 and C_2 are physical constants ($C_1 = 1.191 \times 10^8 W\ \mu m^4 sr^{-1} m^{-2}$, $C_2 = 1.439 \times 10^4\ \mu m\ K$). In case of a flat urban surface, T_r and the complete surface temperature will be the same.

Methods to estimate the land surface emissivity using space-based radiometric data have been summarized by Li et al. (2013). Widely used methods to retrieve emissivity, such as temperature and emissivity separation (TES) or the land cover and normalized difference vegetation index (NDVI) threshold, do not consider urban geometry. Emittance and exitance from a flat surface differ from a geometrically complex urban surface because the multiple reflection and scattering cause a cavity effect. The effective emissivity of an urban canopy must account for geometric effects to estimate T_r, as according to Yang et al. (2015):

$$\varepsilon_\lambda(i)' = \varepsilon_\lambda(i) / \left(1 - \left(1 - \varepsilon_\lambda(i)\right)\left(1 - V(i, \text{sky})\right)\right) \tag{17.5}$$

$V(i, \text{sky})$ represents the sky view factor which determined by building height, building density, and the topography. $V(i, \text{sky})$ can be estimated from urban building data, a Digital Surface Model (DSM), and a Digital Elevation Model (DEM).

The ground-leaving thermal radiance changes with the incorporation of topographic and geometric features in Urban Exitance Models (UEM) which include thermal emittance from all observed facets in a pixel as well as the reflected radiance by all facets. The latter allows to mimic radiometric measurements considering the configuration of the observation and sensor specifications. A Single Channel UEM would then be

$$E(i) = \varepsilon_\lambda(i)' B\left(T_r(i)\right) + \left(1 - \varepsilon_\lambda(i)'\right)\left\{V(i, \text{sky}) * R_{at}^{\downarrow}(i) + V_{adj}(i) * R_{adj}\right\} \tag{17.6}$$

where $\varepsilon_\lambda(i)'B(T_r(i))$ is the emittance of pixel i, $\left(1-\varepsilon_\lambda\left(i\right)'\right)\left\{\left(1-V\left(i,\text{sky}\right)\right)\varepsilon_\lambda\left(i\right)B\left(Ts\left(i\right)\right)+V\left(i,\text{sky}\right)*R_{\text{at}}^{\downarrow}\left(i\right)+V_{\text{adj}}\left(i\right)*R_{\text{adj}}\right)$ is "the fraction of atmospheric emittance and of radiance reflected by adjacent pixels and the facets within pixel i." The $\varepsilon_\lambda(i)'$ is calculated by Eq. (17.5). $V(i, \text{sky})$ is the "Sky View Factor" of pixel i. The "atmospheric downward radiance" and the "mean view factor from adjacent pixels to pixel i" are represented by $R_{\text{at}}^{\downarrow}\left(i\right)$ and $V_{\text{adj}}(i)$. This is used to calculate "the fraction of exitance from adjacent pixels to pixel i, "i.e. impact induced by the neighboring pixels on the target pixel i. R_{adj} is "the mean exitance of adjacent pixels" and is also influenced by the geometry of the urban canopy.

Another two widely used methods to retrieve surface temperature are the split-window (SW) and the TES algorithms. The SW algorithm removes the influence of atmosphere based on the difference in TOA radiance acquired in two adjacent spectral channels with central wavelengths of such as 10.8 and 12 μm. The material emissivity of a flat land surface can be utilized to account for the surface contribution to the difference in the radiance between the two channels. In complex urban areas, the material emissivity cannot be used to separate the effects of urban geometry and atmosphere since the urban geometry changes the contrast between the radiance at the two adjacent spectral channels (Yang et al. 2015).

The spectral contrast in the emittance captured by a multi-spectral imaging radiometer is the key to retrieve surface temperature using the TES algorithm. Both geometry and materials limit the application of TES in urban areas. First, maximum–minimum difference (MMD) relationships have been established by analyzing spectral libraries, which may not include samples on new construction materials used in urban areas, such as metal and glass. For example, metal does not follow this empirical relationship (Payan and Royer 2004). Abundant use of metals in building can induce considerable biases while applying TES. Second, the spectral effective emissivity of urban targets does not necessarily follow any established MMD relationship, which may need to be determined considering site-specific materials and geometry (Yang et al. 2016). Considering that the single-channel method is not affected by the contrast of different spectral bands, the case study in this chapter adopted the single-channel method as an example.

17.2.2 MODELING THE RELATION BETWEEN T_C AND T_R

T_r is more easily available from satellite images than T_c, while T_c is needed for urban climate research. In a nadir viewing thermal image, the radiance emitted and reflected by the horizontal facets but emitted by any facet and atmosphere is observed. The convective and radiative exchange of energy from roads and vertical facets of buildings contributes to determine the surface temperature of horizontal facets (Yang and Li 2015; Nazarian and Kleissl 2015). Thus, the observed T_r is partly associated with T_c and wall temperature. Both T_r and T_c are strongly associated with the height, areal density, and material of buildings as well as micro-climate. Spatial variations in surface temperature are driven by variability in the radiative and connective energy exchange between the wall facets and air within the built-up space as well as shadows of buildings. T_r and T_c are similar over homogenous areas or pure pixels. The difference between T_r and T_c increases with landscape complexity, however, where the energy exchange is governed by the complex geometry of urban features, including density of building and material properties of buildings. To determine the relationship between T_r and T_c we need to take these properties of an urban landscape along with micro-climate conditions into account.

For daytime, the relation between T_r and T_c can be written as:

$$T_c = f_d\left(T_r, \lambda_p, F, Kn, \theta_a, \theta_z, Fv, Hv, \ldots\right) \tag{17.7}$$

where T_r is the radiometric surface temperature (K), λ_p is the building density, F is the ratio of the wall facet area to the area of building footprint which contains the building and the road around it, which is related to the building density and aspect ratio. Kn indicates the solar irradiance above the urban canopy ($W m^{-2}$), θ_a is the solar azimuth angle (°), θ_z is the solar zenith angle (°), Fv is vegetation fraction, and Hv is related to vegetation height. λ_p is related to the area of rooftops, which is directly observed by a nadir imaging radiometer. F is related to wall facet areas, which is the fraction unobserved by a nadir imaging radiometer. Thus, this study incorporates F and λ_p to examines the difference between T_c and T_r.

The relationship between T_c and T_r becomes simpler at nighttime due to elimination of factors associated with solar irradiance:

$$T_c = f_d\left(T_r, \lambda_p, F, Fv, Hv, \ldots\right) \tag{17.8}$$

Generally, more parameters can increase the accuracy in estimating T_c from T_r. Practically, we can only choose a few important and dominant parameters in constructing the relationship between T_c and T_r.

The essential part to estimate T_c from T_r is how to construct the relation between T_c and T_r. Numerical models of urban microclimate can be utilized to generate pseudo-observations of the radiometric surface temperature and of the urban surface facet temperatures. We need to determine T_c, under different geometric and meteorological conditions, and then build the relationship between T_c and T_r. Lastly, this relationship can be used to estimate the T_c from the remotely-sensed T_r. Here, we only show the case without vegetation and applying to nadir-looking radiometer to measure T_r. Here, the pseudo-observations of T_r and T_c were generated under different conditions by using the temperatures of urban facets in 3D model (TUF-3D, see Krayenhoff and Voogt (2007). The relations between T_r and T_c were constructed for a range of values of geometric and meteorological parameters under different conditions. TUF-3D is a validated "micro-scale urban energy balance model" forced by meteorological variables, i.e. solar downward radiation, relative humidity, air temperature, wind direction, and speed to produce 3D patterns of energy exchange (Krayenhoff and Voogt 2007). The surface temperatures of all the facets generated by the TUF-3D can be used to produce T_c. Pseudo-observations of T_r can also be generated by inverting the upward longwave radiation, which includes the radiation emitted by the roofs and roads as well as reflected radiation by rooftops and roads.

Prior to developing the relationship between the geometric and climate variables and $T_c - T_r$, it is mandatory to determine the nature of the relationship, linear or nonlinear, between the variables and the $T_c - T_r$. This can help to explain and model the difference between T_c and T_r.

The T_c and T_r modeled by TUF-3D were applied to develop the relationship between T_c and T_r. Selected variables (λ_p, F, Kn, θ_a, θ_z) were used to determine the T_c from T_r in daytime (Eq. 17.7) and nighttime (Eq. 17.8). The effects of vegetation were neglected, since the fractional abundance of vegetation in the very compact urban areas of Hong Kong. The sensitivity analysis on T_c suggested a logarithmic relation between T_c and F and linear relationships with the other variables. The coefficients in Eq. (17.7) (for day time) and Eq. (17.8) (for night time) were estimated using sets of 6700 and 6500 values of T_c and T_r modeled by TUF-3D using different settings of the

geometric and meteorological variables. The relationships developed in both cases are applicable to the range of different scenarios explored by the numerical experiments. A multi-linear polynomial model (Eq. (17.9) for daytime and Eq. (17.10) for nighttime) was developed to parameterize T_c considering the sensitivity analysis of T_c.

$$T_c = a_1 * T_r + a_2 * \lambda_p + a_3 * \ln F + a_4 * Kn + a_5 * \theta_a + a_6 * \theta_z + a_0 \tag{17.9}$$

and nighttime:

$$T_c = b_1 * T_r + b_2 * \lambda_p + b_3 * \ln(F) + b_0 \tag{17.10}$$

where $a_0 \sim a_6$ and $b_0 \sim b_3$ are regression coefficients. Equations (17.9) and (17.10) are applicable to a wide range of climate and urban conditions.

The relationship (Eq. 17.11) between T_c and T_r obtained by fitting Eq. (17.9) to the model-generated pseudo-observations gave root mean square error (RMSE) = 1.50 K with $r^2 = 0.97$. The constructed semi-empirical model (Eq. 17.11) had larger RMSEs when applied to estimate the T_c at sunrise (8 a.m.) and sunset (5 p.m.). This is because heat convection rather than solar irradiance determines UST, i.e. the effect of geometry is completely different at this time of day, when the difference between T_c and T_r is rather small. During the central part of the day, i.e. when solar irradiance is the main determinant of UST, the model (Eq. 17.11) performed better with RMSE < 1 K. The results of numerical experiments also indicated that the urban geometry is the main determinant of T_c in the afternoon.

In summary, the relationship to estimate T_c from T_r was

$$T_c = 0.913 * T_r - 5.390 * \lambda_p - 1.090 * \ln F + 0.001 * Kn - 0.013 * \theta_a + 0.139 * \theta_z + a_0 \tag{17.11}$$

During nighttime (9 p.m.–6 a.m.), $T_c - T_r$ is much smaller than in daytime. Urban geometry still determines the surface energy exchange and results in uneven cooling, but the physics behind the influence of geometry on UST is different. Like the daytime case, the sensitivity analysis guided the selection of influential variables and building structure parameters to construct the semi-empirical model (Eq. 17.10). The relationship between T_c and T_r applicable to nighttime was

$$T_c = 0.927 * T_r + 3.455 * \lambda_p + 0.184 * \ln(F) + 21.320 \tag{17.12}$$

where $r^2 = 0.98$ and RMSE = 0.690 K.

Figure 17.3 shows the scatter plot between actual and estimated T_c for the daytime and nighttime cases.

In summary, to retrieve an UST useful to observe and understand urban climate, the following procedure applies (Figure 17.4): (i) atmospheric correction should be applied to the radiance observed at TOA to get the radiance at the top of the urban canopy; (ii) the effective emissivity including urban geometry and material information should be used to retrieve the radiometric surface temperature; (iii) T_c should be estimated by determining its relation with T_r; and (iv) use T_c for urban climate research.

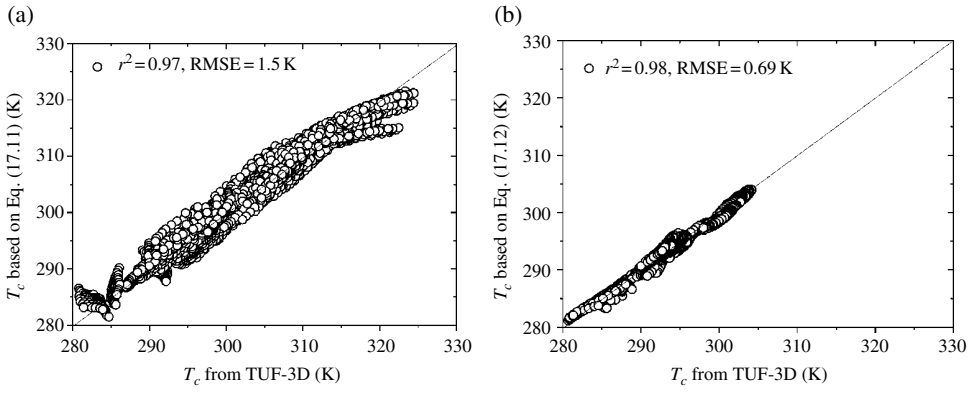

FIGURE 17.3 Actual versus estimated T_c: (a) T_c from Eq. (17.11) (daytime) and (b) T_c from Eq. (17.12) (nighttime).

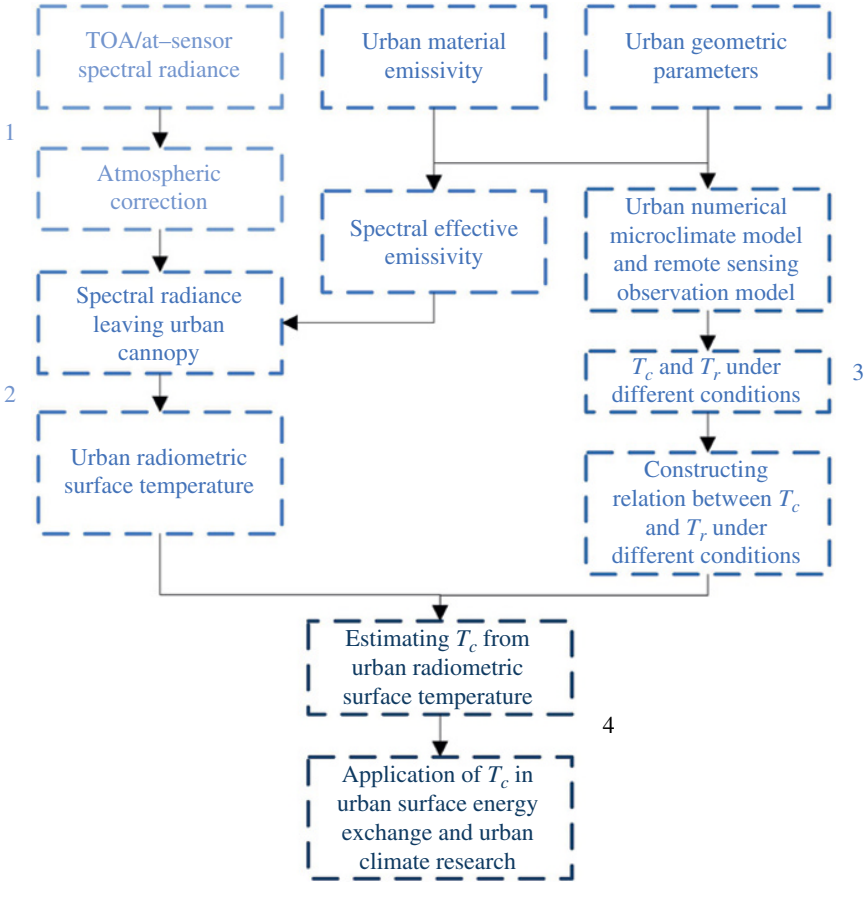

FIGURE 17.4 Workflow to estimate the complete from the radiometric urban surface temperature.

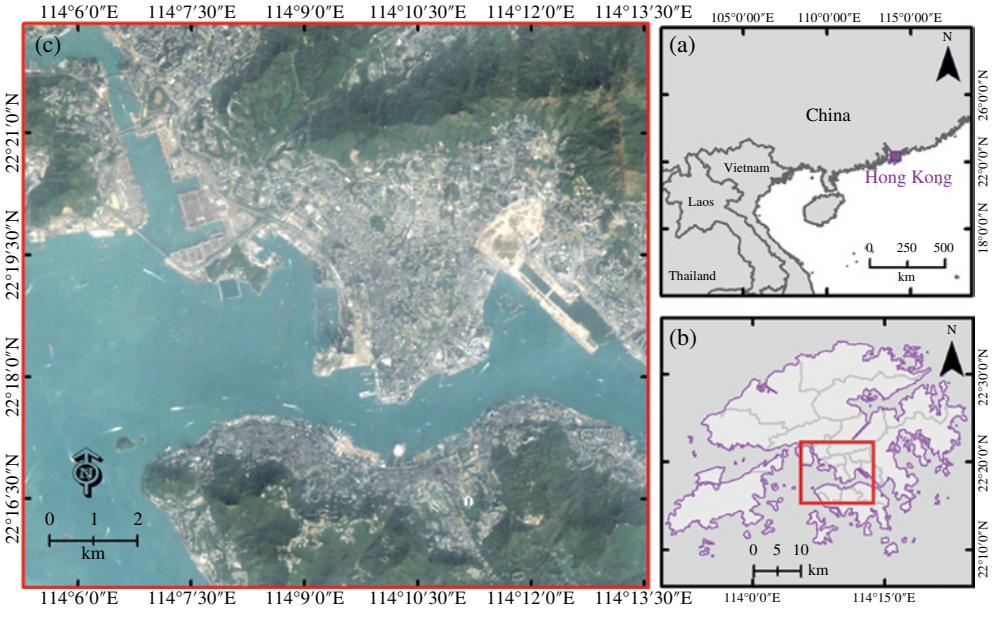

FIGURE 17.5 Location of the study area.

Table 17.1 List of the satellite images used in this study.

Satellite	Date	Local time
Landsat 5	26 March 2010	10:43
	18 September 2010	10:42
	29 October 2010	10:42
	23 December 2010	10:42
ASTER	13 March 2013	22:36
ASTER	4 August 2013	22:36

17.3 STUDY SITE AND DATA

The urban districts of the Kowloon peninsula and Hong Kong Island were selected as study area (Figure 17.5). Hong Kong is a coastal city in South China (22°17′N, 114°09′E), with very compact, high-density built-up space (Chen et al. 2012). Due to this high-rise, high-density urban environment, urban canyons have formed that influence microclimate significantly (Chen et al. 2012). In this condition, the observed radiometric surface temperature cannot represent the real UST.

The thermal images acquired by Landsat 5 TM from 2010 to 2011 and ASTER in 2013 (13 March 2013, 4 August 2013) were used in this study. Table 17.1 shows the observation time and dates of the satellite images used in this study. The building data and DSM data derived by light detection and ranging (LiDAR) with 1 m spatial resolution (Figure 17.6) were collected to map the building height, building height difference, building density, wall area ratio, and sky view factor.

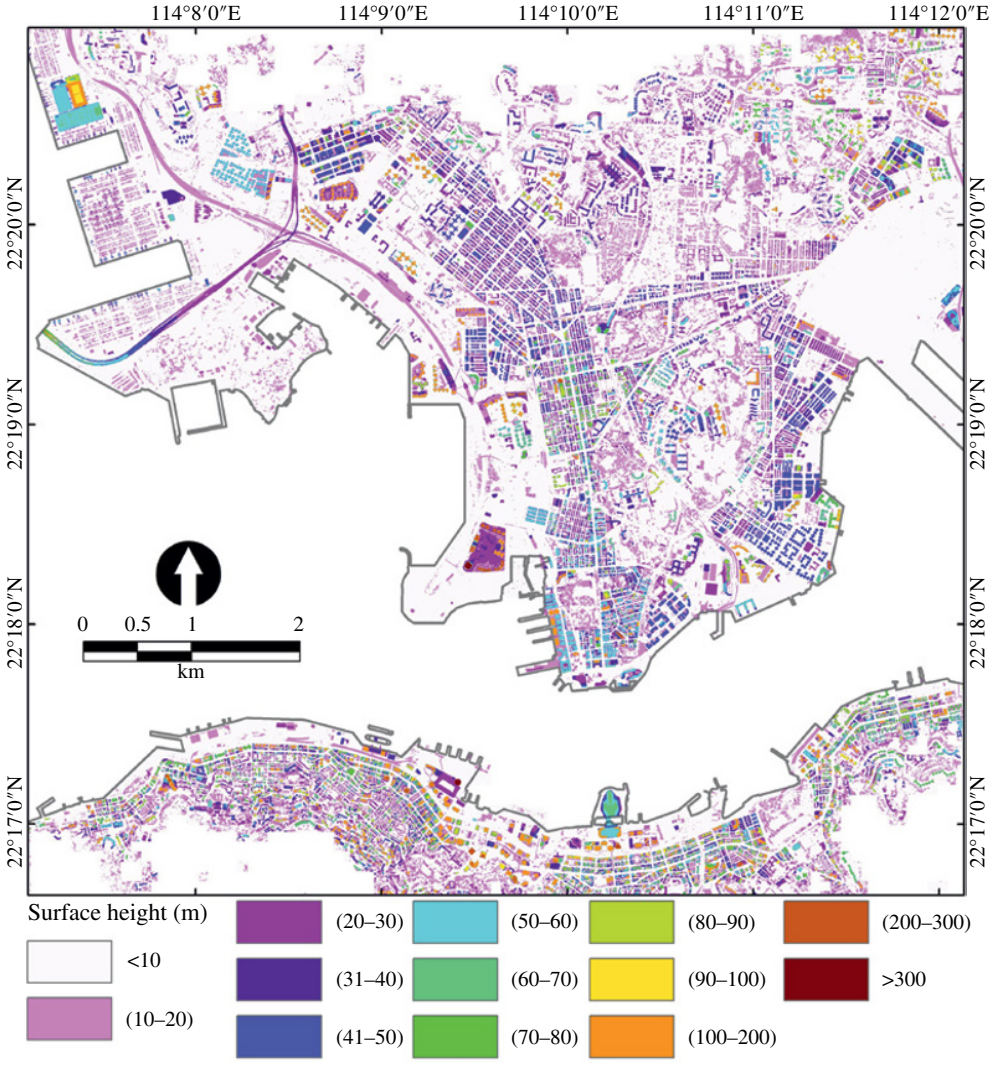

FIGURE 17.6 Building height of the study area.

17.4 RESULTS

17.4.1 RETRIEVAL OF T_R

Figure 17.7 illustrates the retrieved T_r by applying the single channel method to four Landsat 5 TM images acquired in 2010. The results showed that the T_r in the spring and winter (26 March 2010 and 23 December 2010) were lower than that in summer and autumn (18 September 2010 and 29 October 2010). T_r in the built-up areas was lower than that in the open flat impervious areas, especially in the summer season. This is because the shadow effects of buildings make the road and wall temperature are lower than sunlit impervious surface. On the other hand, thermal heterogeneity in summer is greater than in winter. This is because

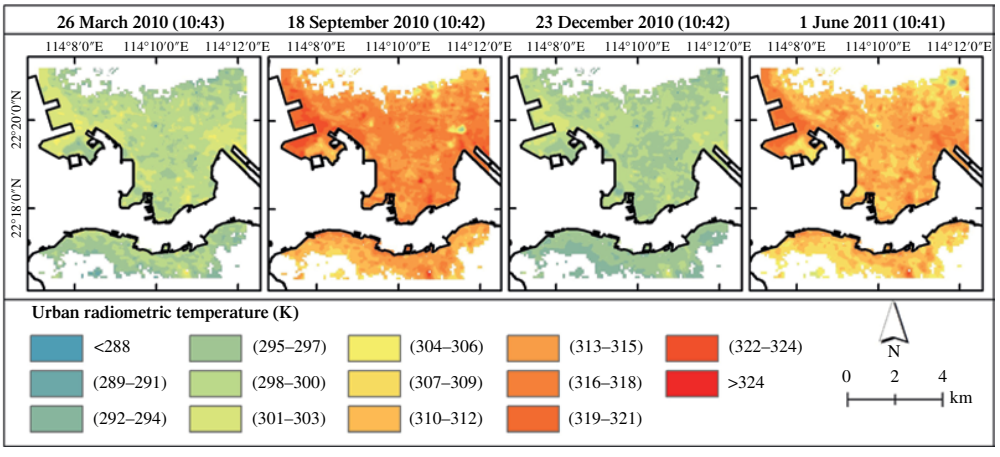

FIGURE 17.7 Surface temperature retrieved by the single-channel method from Landsat 5/TM data in 2010. Note that the ranges of the legends are different.

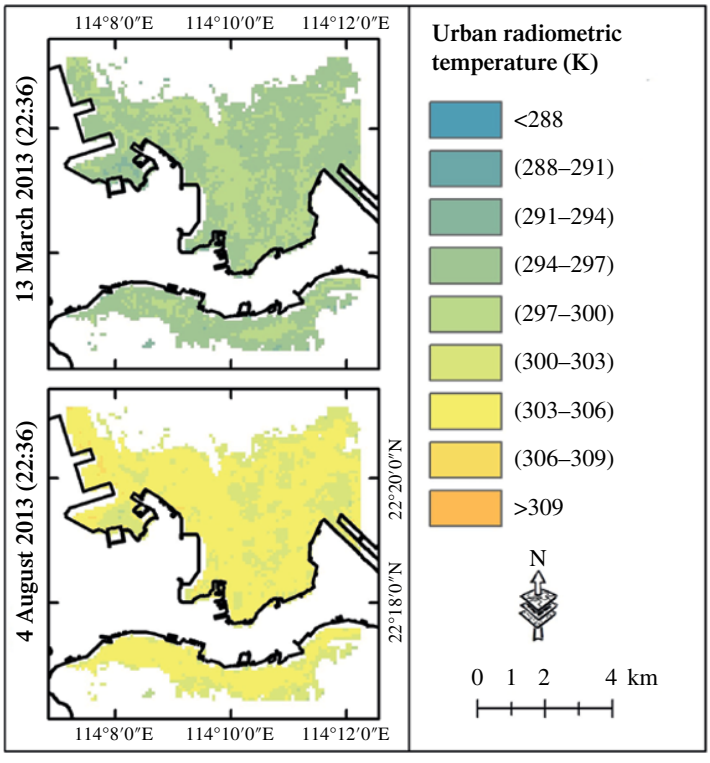

FIGURE 17.8 Surface temperature retrieved by the single-channel method from the ASTER Band 13 data acquired on 13 March 2013 (a) and 4 August 2013 (b). Note that the ranges of the legends are different.

solar radiation in summer is higher than winter and spring, which increases the temperature difference between shadow area and sunlit area. Thermal heterogeneity increases the difficulty of interpreting T_r correctly and the difference between T_r and real UST. Streets and roads are heavily affected by adjacent buildings, thus geometric effects cannot be neglected to retrieve the T_r of streets and roads. T_r mainly contains the information emitted by horizontal surfaces and reflected from horizontal surface but emitted from wall. Thus T_r is different from T_c while T_r can be linked with T_c.

The nighttime T_r was retrieved from ASTER band 13 data (Figure 17.8). The spatial pattern of T_r in nighttime is different from that in daytime. In daytime, T_r in densely built-up areas is lower than in open impervious areas because of the shadow effects. Contrariwise, in nighttime T_r in densely built-up areas is higher than in open areas. ASTER surface temperature products based on TES are available. The ASTER TES algorithm is not applicable in urban areas, since TES is based on spectral libraries on material emissivity. In addition, thermal and material heterogeneity have complex effects on the spectral exitance of urban targets. Particularly, the variability in thermal heterogeneity and materials can result in a different spectral emittance of a composite urban target, with an impact on the UST retrieved with the TES algorithm.

17.4.2 ESTIMATION AND MONITORING OF T_c OVER URBAN AREAS

Daytime (Figure 17.9) and nighttime (Figure 17.10) T_c was estimated by applying Eq. (17.11) and Eq. (17.12) to the T_r retrievals from Landsat TM respectively ASTER image data. Previous findings (Yang et al. 2020) indicated that the semi-empirical model (Eq. 17.11)

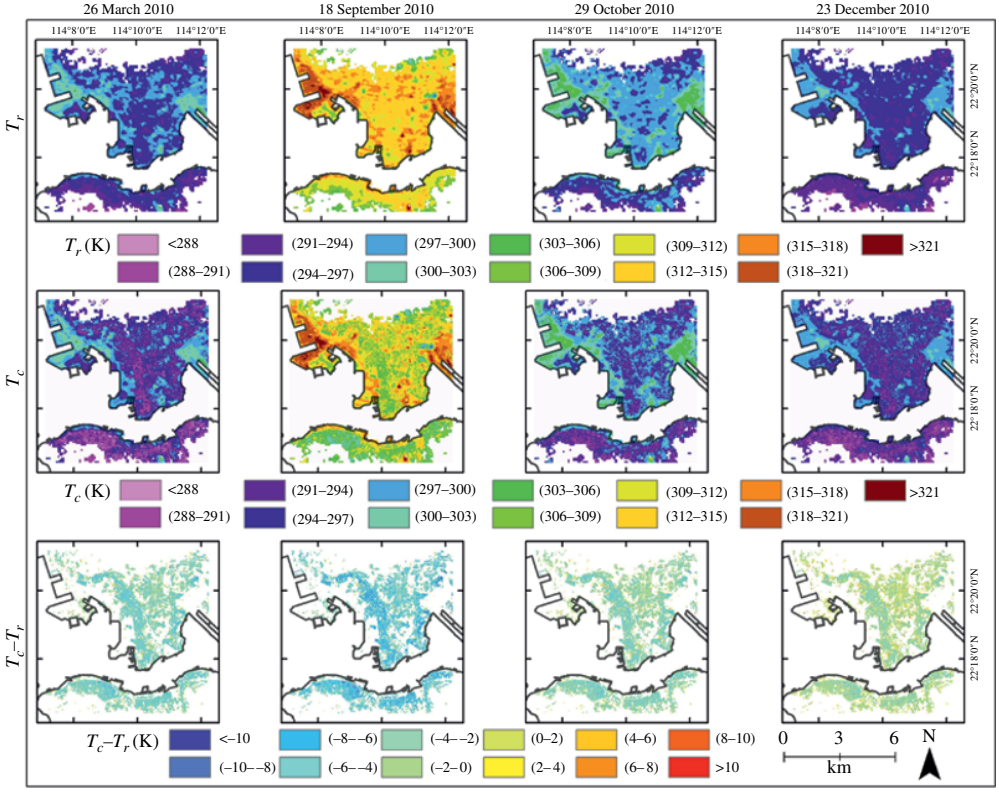

FIGURE 17.9 Daytime, T_r and T_c and their difference $T_c - T_r$ retrieved from the Landsat TM Band 6 data acquired in 2010.

can be used to estimate T_c for compact urban areas without or little vegetation. The results showed that the T_c of flat impervious areas was higher than of areas with high-density buildings (Figure 17.9). In daytime, T_c was generally lower than T_r. The $T_c - T_r$ difference shows a degree of seasonality in response to the seasonal evolution of the solar zenith angle. The mean value of $(T_c - T_r)$ was −2.15 K, while the maximum absolute value reached 6 K in extreme cases in winter, i.e. on 23 December 2010. On 18 September 2010, the mean value of $T_c - T_r$ was −4.98 K, while the maximum absolute value reached 10 K in areas with high-density buildings. In summer, solar irradiance is the dominant driver of spatial heterogeneity of UST, considering that the solar elevation determines the shadows in the urban canyon. The maximum value of $(T_c - T_r)$ appeared on 18 September 2010 since the solar zenith angle of 18 September 2010 was smaller than on the remaining dates of available image data. A smaller solar zenith angle results in temperatures of wall facets lower than that of rooftops because solar irradiance on wall facets is lower. A higher solar zenith angle increases solar irradiance on wall facets, i.e. a larger $(T_c - T_r)$. In summer, T_c was lower than T_r in almost all urban areas. During other seasons, T_c was higher than T_r in several built-up areas with lower building density and fewer high-rise buildings. Because of higher solar zenith angle and less blockage by buildings, solar irradiance on wall facets is higher under these conditions.

Radiometric surface temperature retrieved from ASTER-TIR data was used to estimate nighttime T_c based on Eq. (17.12) and building data. During nighttime, T_c was higher than T_r in built-up areas (Figure 17.10), with the difference between T_c and T_r reaching 2 K (Figure 17.10). The $(T_c - T_r)$ during nighttime in spring was higher than in summer, which is contrary to daytime. The mean value of $(T_c - T_r)$ during the summer nighttime (4 August 2013) was −0.21 K, while in a spring nighttime (13 March 2013) was 0.30 K. In high-density built-up areas, T_c was higher than T_r during the nights of both 13 March 2013 and 4 August 2013. This is because heat dissipation by rooftop facets is larger than wall or street facets in nighttime. The dominant land surface process at nighttime is radiative and convective dissipation. Rooftop facets are more efficient in radiative and convective dissipation than wall and street facets, which may result in a lower rooftop surface temperature than wall and street surface temperatures in the late evening. The rooftop surface temperature is likely to determine the T_r observed by a nadir looking TIR imaging radiometer over high-density built-up areas.

During nighttime, the daytime heat storage and nighttime heat dissipation of wall facets are important drivers of the difference between T_r and T_c. The solar zenith angle during daytime on 13 March 2013 was larger than on 4 August 2013, thus solar irradiance on vertical wall facets was higher than in August. This resulted in increasing heat storage at wall facets at daytime. In addition, a compact built-up space reduces both radiative and convective dissipation by wall facets. This means that wall facet temperature will be higher than roof surface temperature at night. In summer, solar irradiance on wall facets is less than on roof facets. This increases the thermal heterogeneity during the summer daytime. Moreover, rooftop temperature decreases faster than wall temperature after sunset, which tends to reduce thermal heterogeneity during nighttime as observed by comparing our images in summer and spring. At night wall facet temperature on 4 August 2013 was lower than rooftop temperature in some areas. Moreover, T_c was lower than T_r in areas with lower building density. In spring and winter, the solar zenith angle is larger than summer, i.e. irradiance on vertical wall facets is larger in spring and winter. Thus, in a winter nighttime, the wall facet temperature is higher than rooftop temperature, while in a summer nighttime the wall facet temperature is slightly higher than the roof surface temperature.

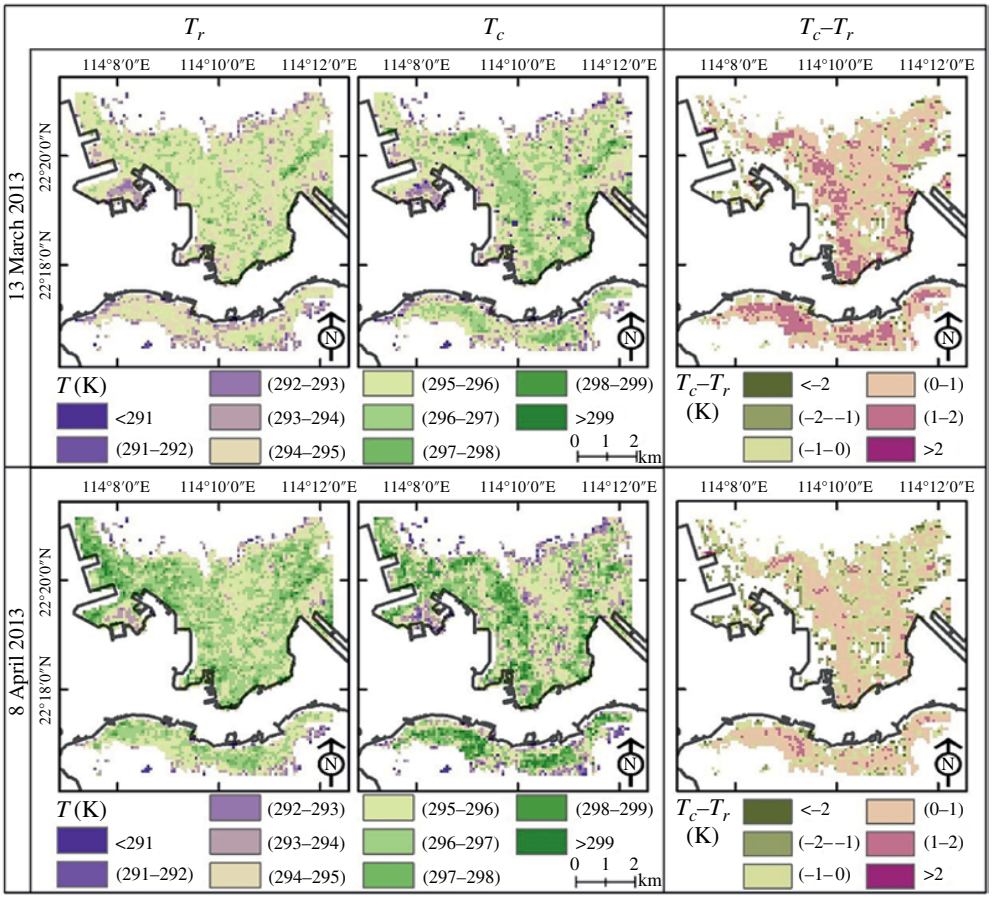

FIGURE 17.10 Nighttime T_r and T_c estimated by applying Eq. (17.10) to the ASTER image data and GIS building data in 2013.

17.5 DISCUSSION AND CONCLUSIONS

The complex urban geometric and material properties limit the observation of thermal remote sensing, and further affect the applicability of thermal infrared remote sensing for urban climate research. If these properties are not considered, the retrieved UST would not have any clear physical meaning when the current algorithms to retrieve surface temperature, such as single-channel, SW, and TES algorithms, are directly used for UST retrieval. The thermal heterogeneity of the urban space determines the thermal anisotropy and radiative fluxes in mixed pixels. In addition, nadir-viewing imaging radiometers cannot capture the emittance of all urban facets because of the obstruction by buildings. Because of these factors, the observed radiometric surface temperature is different from the real urban complete surface temperature, of which the latter is needed for urban surface process and urban climate research. Thus, we should obtain the real urban complete surface temperature for urban climate research. This chapter used a simple case-study to illustrate these concepts and relevant methods in estimating the complete surface temperature.

We firstly examined the limitations of three current most popular surface temperature retrieval methods for radiometric surface temperature retrieval. The SW algorithms rely on the difference of the radiances at 11 and 12 μm. The TES algorithm also uses spectral radiance at multiple wavelengths to separate the emissivity and surface temperature. The complex geometric characteristics and material properties of the urban canopy modify the spectral signature of heterogeneous urban targets, thus increasing the complexity of applying algorithms using multiple spectral bands. The single-channel method only needs one thermal bands, and thus it is more robust than SW and TES to retrieve UST. In any case, the requirements for accurate atmospheric and material properties may also reduce the accuracy of the single-channel method.

The thermal heterogeneity within a mixed pixel can significantly affect the exitance measured by a remote sensor above the urban canopy, and thus radiative exchanges within mixed pixels should be considered to retrieve accurate and meaningful surface temperature. The spatial resolution of satellite TIR data is relatively low to resolve the component of mixed pixels, which makes the retrieved urban radiometric surface temperature not equal to real UST (i.e. complete surface temperature), but they can be linked by using an urban energy exchange model.

Complete surface temperature contains the information on all facets of the built-up space. Thus, complete surface temperature is more representative and meaningful than directional radiometric surface temperature for urban climate research. Observations of thermal infrared exitance convey relevant information over an urban canopy. These observations are affected by urban geometry and material heterogeneity since they determine urban energy exchanges. Space- and airborne nadir-viewing imaging radiometers cannot capture emittance by all facets because of urban geometry. However, these measurements can be linked to the complete surface temperature by combining urban geometry and material information with an urban micro-climate model of energy exchange. The complete surface temperature can then be estimated to study the urban climate and urban heat fluxes.

We then used a simple case study to demonstrate the methodology discussed above, which was based on the estimation of T_c from satellite TIR data under the condition that the urban areas have no vegetation or negligible vegetation. The micro-climate numerical model, TUF-3D, was adopted to simulate T_c and T_r under a wide range of controlled and different conditions. We applied these simulated data to evaluate how different urban geometry and meteorological variables determine the relationship between T_c and T_r in daytime and nighttime. The results showed that the urban geometric and atmospheric properties have different impacts on the difference between T_c and T_r in daytime and nighttime. Numerical experiments by an urban micro-climate numerical model were very effective toward a better understanding of these relationships. Particularly, an urban micro-climate models can be used to understand the relationship between T_c and observed T_r, although the numerical micro-climate model used in this case study, i.e. TUF-3D, can only handle simple building arrays. The buildings in the real world have different shapes and spatial arrangements and these factors determine surface energy exchanges and the pattern in surface temperature. The validation of UST is difficult because of the high thermal heterogeneity. In our case study, the validation was only based on model data. The validation in the real world still needs to be conducted carefully in the near future. In addition, the simple case study did not include vegetation effects. The interaction between buildings and vegetation can be complex because of the totally different thermal properties and different structure and spatial distribution. For example, the UST can be reduced by vegetation evapotranspiration. On the other hand, vegetation cover can also decrease the wind speed and limit heat dissipation, which is not beneficial for UST. These complex land surface processes control the land surface temperature, given the land and meteorological conditions. In addition, the TUF-3D model cannot deal with complex building arrangements and structures as in the real world. For other

more complex conditions with vegetation and different buildings, a different numerical urban climate (e.g. environment for visualizing images (ENVI)-met) and 3D radiative transfer models (e.g. discrete anisotropic radiative transfer [DART]) may be useful. An urban numerical climate model combined with a remote sensing observation model can be an applicable method to construct the relationship between the radiance captured by space- and airborne imaging radiometers and real or complete UST.

It should be noted that our case study is just a simple example of the estimation of T_c from nadir observations of the radiometric surface temperature. Off-nadir observations of T_r come closer to observe T_c, since such observations can capture the emittance by wall facets (Jiang et al. 2018). Currently, only SENTINEL-3 SLSTR (Sea and Land Surface Temperature Radiometer) can provide bi-angular thermal infrared image data. The data record of the AATSR (Advanced Along Track Scanning Radiometer) series instruments also can provide dual-angular thermal images before 2012. Although only providing off-nadir data at low spatial resolution (>1 km), they still provide an opportunity to estimate the complete surface temperature of urban areas.

It is difficult to obtain detailed material information on the urban landscape. Although the dominant driver of UST is building structure and geometric characteristics (Krayenhoff and Voogt 2016), material characteristics can still have significant impacts on component surface temperatures. Our case study used predefined material parameters provided by spectral libraries on urban materials and urban micro-climate models to include the urban material information into the relationship between T_c and T_r. Accurate information on material properties in urban areas cannot be retrieved from satellite data. The approach applied mitigates this problem, while it remains preferable to use local knowledge on material properties. The case study only included the condition that thermal variation is caused by buildings within a pixel, while buildings in neighboring pixels may also cause the spatial variability of temperature by shadowing effect and interference on heat convection, which also needs further exploration.

Overall, the application of thermal remote sensing data for urban climate research is much more complex than for flat natural surface because of the complex geometric and material properties, and therefore it is needed to apply a model of urban micro-climate, as demonstrated by our case study. While we herewith only present a simple case study for UST retrieval, many challenges need to be addressed in the future for improving the applicability of thermal infrared remote sensing in urban areas.

ACKNOWLEDGMENTS

The research reported in this chapter was supported by the National Natural Science Foundation of China (Grant Nos. 41671430, 41901283, 41571366, 61976234, and 61601522) and the MOST High-Level Foreign Expert program (Grant No. G20190161018).

REFERENCES

Adderley, C., Christen, A. & Voogt, J. A. (2015). The effect of radiometer placement and view on inferred directional and hemispheric radiometric temperatures of an urban canopy. *Atmospheric Measurement Techniques*, 8, 2699–2714.

Allen, M., Voogt, J. & Christen, A. (2018). Time-continuous hemispherical urban surface temperatures. *Remote Sensing*, 10, 3.

Arnfield, A. J. (2003). Two decades of urban climate research: A review of turbulence, exchanges of energy and water, and the urban heat island. *International Journal of Climatology*, 23, 1–26.

Becker, F. & Li, Z. L. (1995). Surface temperature and emissivity at various scales: Definition, measurement and related problems. *Remote Sensing Reviews*, 12, 225–253.

Chen, L., Ng, E., An, X., Ren, C., Lee, M., Wang, U. & He, Z. (2012). Sky view factor analysis of street canyons and its implications for daytime intra-urban air temperature differentials in high-rise, high-density urban areas of Hong Kong: A GIS-based simulation approach. *International Journal of Climatology*, 32, 121–136.

Hu, L. & Brunsell, N. A. (2013). The impact of temporal aggregation of land surface temperature data for surface urban heat island (SUHI) monitoring. *Remote Sensing of Environment*, 134, 162–174.

Jiang, L., Zhan, W., Voogt, J., Zhao, L., Gao, L., Huang, F., Cai, Z. & Ju, W. (2018). Remote estimation of complete urban surface temperature using only directional radiometric temperatures. *Building and Environment*, 135, 224–236.

Kanda, M., Kawai, T. & Nakagawa, K. (2005). A simple theoretical radiation scheme for regular building arrays. *Boundary-Layer Meteorology*, 114, 71–90.

Kanda, M., Kanega, M., Kawai, T., Moriwaki, R. & Sugawara, H. (2007). Roughness lengths for momentum and heat derived from outdoor urban scale models. *Journal of Applied Meteorology and Climatology*, 46, 1067–1079.

Krayenhoff, E. S. & Voogt, J. (2007). A microscale three-dimensional urban energy balance model for studying surface temperatures. *Boundary-Layer Meteorology*, 123, 433–461.

Krayenhoff, E. S. & Voogt, J. A. (2016). Daytime thermal anisotropy of urban neighbourhoods: Morphological causation. *Remote Sensing*, 8, 108.

Li, N. & Li, X. (2020). The impact of building thermal anisotropy on surface urban heat island intensity estimation: An observational case study in Beijing. *IEEE Geoscience and Remote Sensing Letters*, 17, 2030–2034.

Li, Z. -L., Tang, B. -H., Wu, H., Ren, H., Yan, G., Wan, Z., Trigo, I. F. & Sobrino, J. A. (2013). Satellite-derived land surface temperature: Current status and perspectives. *Remote Sensing of Environment*, 131, 14–37.

Morrison, W., Kotthaus, S., Grimmond, C. S. B., Inagaki, A., Yin, T., Gastellu-Etchegorry, J.- P., Kanda, M. & Merchant, C. J. (2018). A novel method to obtain three-dimensional urban surface temperature from ground-based thermography. *Remote Sensing of Environment*, 215, 268–283.

Nazarian, N. & Kleissl, J. (2015). CFD simulation of an idealized urban environment: Thermal effects of geometrical characteristics and surface materials. *Urban Climate*, 12, 141–159.

Nazarian, N., Martilli, A. & Kleissl, J. (2018). Impacts of realistic urban heating, part I: Spatial variability of mean flow, turbulent exchange and pollutant dispersion. *Boundary-Layer Meteorology*, 166, 367–393.

Oke, T. R. (1982). The energetic basis of the urban heat island. *Quarterly Journal of the Royal Meteorological Society*, 108, 1–24.

Oke, T. (1988). The urban energy balance. *Progress in Physical geography*, 12, 471–508.

Oke, T., Mills, G., Christen, A. and Voogt, J. (2017). Urban Climates. ISBN: 978-1-107-42953-6. DOI: 10.1017/9781139016476.

Payan, V. and Royer, A., 2004. Analysis of temperature emissivity separation (TES) algorithm applicability and sensitivity. *International Journal of Remote Sensing*, 25(1): 15–37.

Rizwan, A. M., Dennis, L. Y. & Liu, C. (2008). A review on the generation, determination and mitigation of urban heat island. *Journal of Environmental Sciences*, 20, 120–128.

Roth, M., Oke, T. R. & Emery, W. J. (1989). Satellite-derived urban heat islands from three coastal cities and the utilization of such data in urban climatology. *International Journal of Remote Sensing*, 10, 1699–1720.

Voogt, J. A. & Grimmond, C. (2000). Modeling surface sensible heat flux using surface radiative temperatures in a simple urban area. *Journal of Applied Meteorology*, 39, 1679–1699.

Voogt, J. A. & Oke, T. R. (1997). Complete urban surface temperatures. *Journal of Applied Meteorology*, 36, 1117–1132.

Voogt, J. A. & Oke, T. (1998). Effects of urban surface geometry on remotely-sensed surface temperature. *International Journal of Remote Sensing*, 19, 895–920.

Voogt, J. A. & Oke, T. R. (2003). Thermal remote sensing of urban climates. *Remote Sensing of Environment*, 86, 370–384.

Wang, D. & Chen, Y. (2019). A geometric model to simulate urban thermal anisotropy in simplified dense neighborhoods (GUTA-dense). *IEEE Transactions on Geoscience and Remote Sensing*, 57, 6226–6239.

Wang, D., Chen, Y. & Zhan, W. (2018). A geometric model to simulate thermal anisotropy over a sparse urban surface (GUTA-sparse). *Remote Sensing of Environment*, 209, 263–274.

Xu, W., Wooster, M. & Grimmond, C. (2008). Modelling of urban sensible heat flux at multiple spatial scales: A demonstration using airborne hyperspectral imagery of Shanghai and a temperature–emissivity separation approach. *Remote Sensing of Environment*, 112, 3493–3510.

Yang, X. & Li, Y. (2015). The impact of building density and building height heterogeneity on average urban albedo and street surface temperature. *Building and Environment*, 90, 146–156.

Yang, J., Wong, M. S., Menenti, M. & Nichol, J. (2015). Modeling the effective emissivity of the urban canopy using sky view factor. *ISPRS Journal of Photogrammetry and Remote Sensing*, 105, 211–219.

Yang, J., Wong, M. S., Menenti, M., Nichol, J., Voogt, J., Krayenhoff, E. S. & Chan, P. W. (2016). Development of an improved urban emissivity model based on sky view factor for retrieving effective emissivity and surface temperature over urban areas. *ISPRS Journal of Photogrammetry and Remote Sensing*, 122, 30–40.

Yang, J., Wong, M. S., Ho, H. C., Krayenhoff, E. S., Chan, P. W., Abbas, S. & Menenti, M. (2020). A semi-empirical method for estimating complete surface temperature from radiometric surface temperature, a study in Hong Kong city. *Remote Sensing of Environment*, 237, 111540.

Zhan, W., Chen, Y., Voogt, J. A., Zhou, J., Wang, J., Ma, W. & Liu, W. (2012). Assessment of thermal anisotropy on remote estimation of urban thermal inertia. *Remote Sensing of Environment*, 123, 12–24.

View publication stats